Chapter 4

Skin of Atopic Dermatitis patients shows disturbed β-glucocerebrosidase and acid sphingomyelinase activity that relates to changes in stratum corneum lipid composition

Skin of Atopic Dermatitis patients shows disturbed β-glucocerebrosidase and acid sphingomyelinase activity that relates to changes in stratum corneum lipid composition

D.E.C. Boer, J. van Smeden, H. Al-Khakany, E. Melnik, R. van Dijk, S. Absalah, R. J. Vreeken, C.C.P. Haenen, A.P.M. Lavrijsen, H.S. Overkleeft, J.M.F.G Aerts, J.A. Bouwstra.

Abstract

Patients with Atopic Dermatitis (AD) suffer from inflamed skin and skin barrier defects. Proper formation of the outermost part of the skin, the stratum corneum (SC), is crucial for the skin barrier function. In this study we analyzed the localization and activity of lipid enzymes β-glucocerebrosidase (GCase) and acid sphingomyelinase (ASM) in the skin of AD patients and controls. Localization of both the expression and activity of GCase and ASM in the epidermis of AD patients was altered, particularly at lesional skin sites. These changes aligned with the altered SC lipid composition. More specifically, abnormal localization of GCase and ASM related to an increase in specific ceramide subclasses [AS] and [NS]. Moreover we related the localization of the enzymes to the amounts of SC ceramide subclasses and free fatty acids (FFAs).

We report a correlation between altered localization of active GCase and ASM and a disturbed SC lipid composition. Localization of antimicrobial peptide beta-defensin-3 (HBD-3) and AD biomarker Thymus and Activation Regulated Chemokine (TARC) also appeared to be diverging in AD skin compared to control. This research highlights the relation between correct localization of expressed and active lipid enzymes and a normal SC lipid composition for a proper skin barrier.

Introduction

Atopic Dermatitis (AD) is a multifactorial disease in which both immunological aspects and skin barrier defects contribute to clinical manifestations as erythema, xerosis and pruritis. The interplay between inflammation and skin barrier in this disease is complex, and it is hypothesized that a skin barrier dysfunction may facilitate exogenous compounds (e.g. pathogens, allergens) to penetrate the skin and provoke an immune response [1]. Subsequently,

this immune response may also affect the barrier properties of the skin. This is also known as the "outside–inside–outside" model of AD pathogenesis [2, 3]. Nonetheless, AD is known to be a heterogeneous disease that can be driven by activation of the adaptive immune response, along with being the initiator that activates key TH1, TH17 and TH22 cytokine pathways [4].

The strongest predisposing factor for developing AD is loss-of-function mutations in the *filaggrin* gene (*flg*) [5, 6]. The protein filaggrin is an essential component for a proper formation of the Stratum Corneum (SC), the outermost skin layer that functions as the primary physical skin barrier. The SC is the non-vital final keratinocyte differentiation product forming the outermost layer of the skin. It consists of multiple layers of corneocytes (dead cells) embedded in an extracellular lipid matrix and plays an eminent role in the barrier function of the skin. The breakdown products of filaggrin – forming a substantial part of the natural moisturizing factor (NMF) – are essential for water retention in theSC. Additionally, the NMF is important for maintaining a physiologic acidic environment in the SC, supporting an optimal skin-pH and water level for proper enzyme activity in the skin [7, 8]. Several of these skin enzymes play a crucial role in generating key barrier components of the SC, the SC lipids, which form a highly ordered intercellular matrix [9, 10]. The composition of the SC lipid matrix is crucial for a proper skin barrier, and changes in these lipids are related to several skin barrier diseases [11, 12]. The main SC lipids are ceramides, free fatty acids (FFAs) and cholesterol. Ceramide synthases are essential for the formation of ceramides *de novo*. To store the ceramides in the viable cells, the ceramides are converted to glucosylceramides and sphingomyelin by the enzymes glucosylceramide synthase and sphingomyelin synthase, respectively (as reviewed in [13]). Besides ceramides also free fatty acids (FFAs)

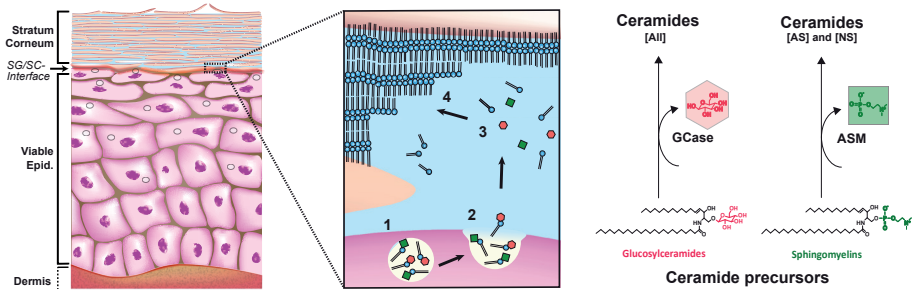

Figure 1: Schematic overview of formation SC lipid layers at the SG/SC-interface. 1. Lamellar Bodies (LBs) in the keratinocytes are filled with ceramide precursors glucosylceramides and sphingomyelins together with the enzymes GCase and ASM. 2. Extrusion process of the lipids and lipid enzymes. 3. Conversion of glucosylceramides and sphingomyelins by respectively GCase and ASM to ceramides. 4. Formation of the extracellular stacked lipid layers: the lipid barrier in the SC.

reside in the lipid matrix of the SC. Proper expression of stearoyl CoA desaturase (SCD) and ELOVL1-7 (elongation of very long chain fatty acids 1–7) have been shown to be key for a proper FFA and ceramide composition [13]. An impaired skin barrier is typically monitored by an increased transepidermal water loss (TEWL. AD patients suffer from an increased TEWL (reduced skin barrier). This increased TEWL is correlated to changes in the SC lipids, particularly in two key classes: the ceramides, and their precursors the FFAs [14]. Whereas FFAs contain a single acyl chain, ceramides contain two long chains attached to one polar head group. In SC both the head group and carbon chain length show a wide variation in molecular architecture [15]. To distinguish all SC ceramides, they are categorized in subclasses based on their architecture, illustrated in Supplemental Figure 1. The SC ceramide composition in AD patients is changed. Compared to control skin, lesional AD skin demonstrates a significant decrease in the average carbon chain length of both ceramides and FFAs [16-18]. In addition, a (relative) increase in [AS] and [NS] ceramides in lesional skin has been observed [19-21]. The reason why particularly ceramides [AS] and [NS] are increased in barrier disrupted skin is not fully understood, but likely originates from changes in the epidermal biosynthesis of the SC ceramides [12, 22].

A pivotal step in this ceramide conversion is the final process in which ceramide precursors – glucosylceramides and sphingomyelins – are extruded from the Stratum Granulosum (SG) keratinocytes into the extracellular environment at the SG/SC interface [14]. During this extrusion process of lipids and their corresponding enzymes, the ceramide precursors transform into their final barrier constituents. Here, glucosylceramides and sphingomyelins are converted by respectively β-glucocerebrosidase (GCase) and acid sphingomyelinase (ASM) (Figure 1). Both GCase and ASM will convert their substrates into ceramides, but conversion by ASM will lead to only ceramide subclasses [AS] and [NS], whereas ceramide formation via GCase may lead to ceramides of any subclass [23, 24]. It is known that the expression of these enzymes is mildly changed in the epidermis of some AD subjects, particular at lesional skin sites [25-27]. However, not all reported changes in the SC ceramides in AD patients could be explained by the expression of GCase and ASM [28]. Literature suggests that micro-environmental factors like SC water content and local skin-pH are essential for proper activity (besides expression) of these enzymes [29, 30]. The skin microbiome and inflammation are changed in AD [31-33] and could therefore consequently have an effect on the SC lipid composition. This has not been studied previously, thus we additionally examined the localization of Human beta defensing (HBD)-3 as a readout for the microbiome, plus it has been reported to be decreased in AD. Furthermore we included Thymus and Activation Regulated Chemokine (TARC), which is

involved in Th2 cell migration and has been confirmed as a biomarker for AD severity [32, 33]. This also provides the opportunity to research whether the localization of these AD markers change concordantly with GCase and ASM localization.

We visualized *in situ* enzyme expression and activity of GCase and ASM in human skin tissue of AD subjects and controls and analyzed the SC ceramides and FFas by LC/MS. In addition, we examined several AD markers (both locally and systemically) to study the relationship between the SC lipids and the inflammatory aspects, as it is known that cytokines may induce lipid abnormalities in atopic skin [34, 35]. Our findings elucidate the relation between localization of – particularly active – GCase and ASM, versus the SC lipid composition. In addition, this study elaborates on the clinical relevance by relating these enzymes and SC lipid composition to biologically/clinically important parameters like TEWL and disease severity scores [36].

Results

This study cohort consisted of ten patients diagnosed with AD and five controls. Three AD patients had lesional regions on their arms during the study period. A summary of the results with respect to (local) SCORAD, EASI, TEWL and skin-pH per time point is provided in figure 2. In agreement with previous studies, our AD cohort demonstrated an elevated baseline TEWL for non-lesional as well as lesional skin regions in comparison to control skin [37]. In addition, skin-pH values were in similar ranges as reviewed elsewhere [38]. These general parameters support the representativeness of this AD cohort in relation to established literature [37-40].

Location of expressed enzyme does not predict the location of active enzyme.

We first studied the localization of GCase expression in the skin cryosections of the control subjects. The top panel in figure 3 shows the expression of GCase mainly concentrated at the interface between the viable epidermis and SC (SG/SC-interface). Active GCase was visualized using the activity based probe MDW941. Concerning the intensity of the signal, a substantial intra- and inter-individual variation was observed. Therefore, we focused on the location of the activity in this study (supplemental figure S2). In all controls, the active enzyme was primarily observed in the SC, no active GCase was observed in the viable epidermis. Active GCase was present in the SC lipid matrix surrounding the corneocytes: either throughout all SC layers, or in the lower regions of the SC. Note that the signal intensity is very heterogeneous between subjects and even within a single skin section, but localization remains in the SC lipid matrix for all controls.

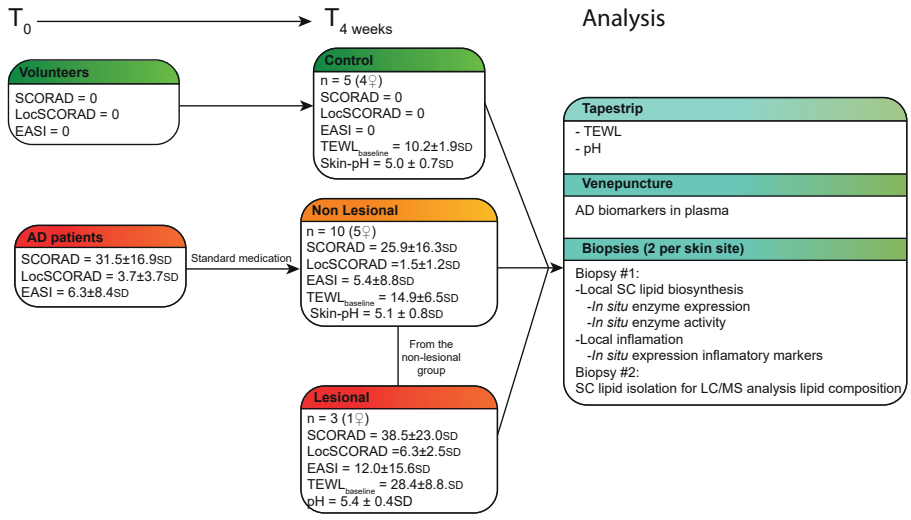

Figure 2: Schematic overview experimental set up and scoring of the cohort. T_0: SCORAD and EASI parameters of volunteers and AD patients. T_4 weeks: SCORAD, EASI, TEWL and pH parameters of controls and AD patients. Skin samples from arm regions and two biopsies were taken from all subjects. From 3 AD patients non-lesional and lesional skin samples were taken. Furthermore venipuncture and tape stripping was performed.

When focusing on ASM expression in the control skin sections, the expression was present throughout the viable epidermis. The activity of ASM was determined by zymography. The intensity of this signal was also very heterogeneous, even within a single skin cryosection of a subject. In one subject (nr. 5) no ASM activity was detected. The location of ASM activity was detected mainly in the lower layers of the SC near the SG/SC-interface or scattered throughout the whole SC, but no activity signal was encountered in the viable epidermis.

Location of expressed enzyme does not predict the location of active enzyme.

We first studied the localization of GCase expression in the skin cryosections of the control subjects. The top panel in figure 3 shows the expression of GCase mainly concentrated at the interface between the viable epidermis and SC (SG/SC-interface). Active GCase was visualized using the activity based probe MDW941. Concerning the intensity of the signal, a substantial intra- and inter-individual variation was observed. Therefore, we focused on the location of the activity in this study (supplemental figure S2). In all controls, the active enzyme was primarily observed in the SC, no active GCase was observed in the viable epidermis. Active GCase was present in the SC lipid matrix surrounding the corneocytes: either throughout all SC layers, or in the lower regions of the SC. Note that the signal intensity is very heterogeneous between subjects and

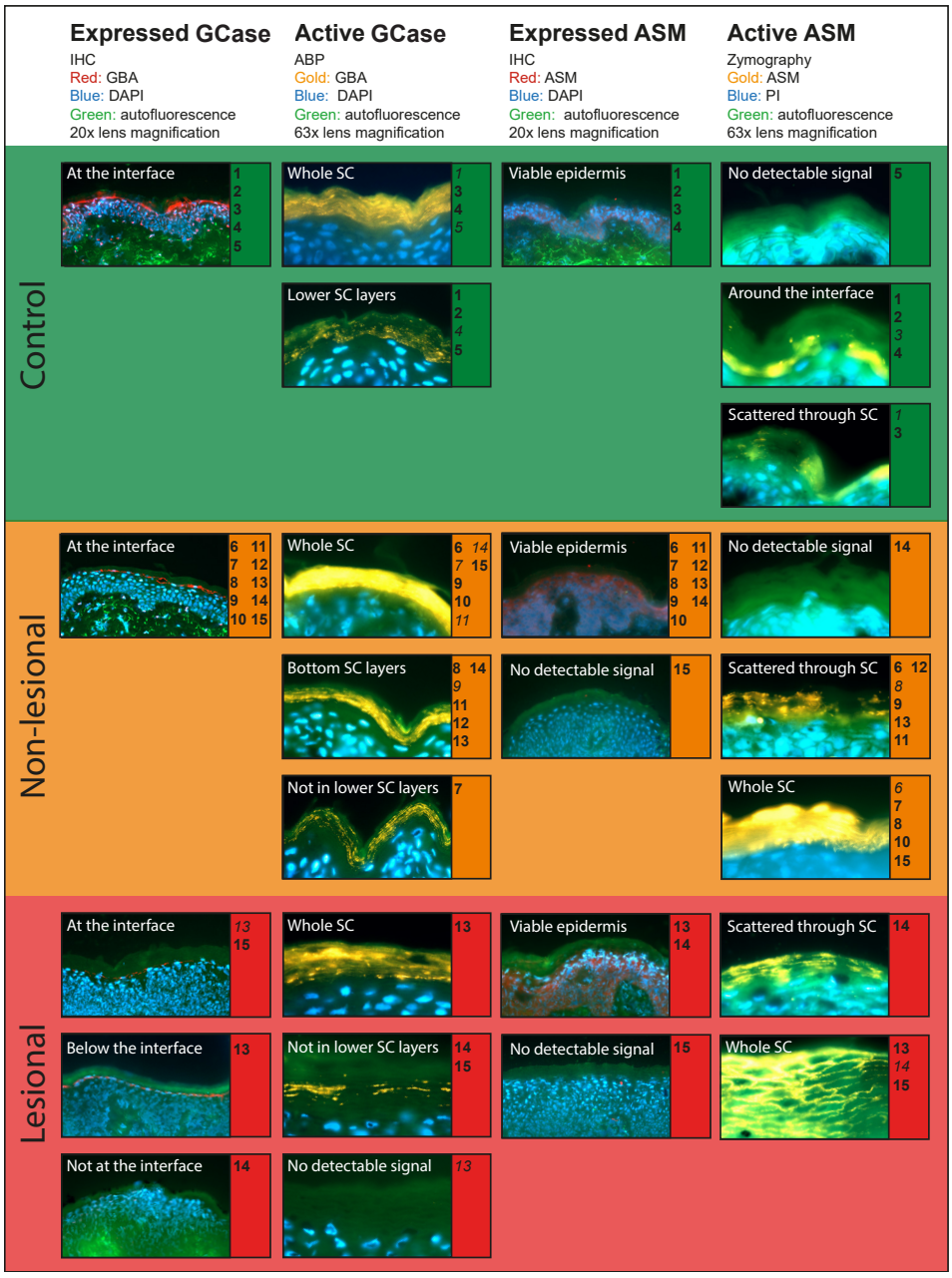

Figure 3: *In situ* expression and activity localization of GCase and ASM within skin sections of control, non-lesional AD and lesional AD skin. Microscopy images showing in which skin layers expressed and active enzymes are localized. Depicted are which localization patterns can be found in each subject. Bold numbers show its main occurrence per subject. Italic numbers demonstrate the less abundant patterns.

even within a single skin section, but localization remains in the SC lipid matrix for all controls.

When focusing on ASM expression in the control skin sections, the expression was present throughout the viable epidermis. The activity of ASM was determined by zymography. The intensity of this signal was also very heterogeneous, even within a single skin cryosection of a subject. In one subject (nr. 5) no ASM activity was detected. The location of ASM activity was detected mainly in the lower layers of the SC near the SG/SC-interface or scattered throughout the whole SC, but no activity signal was encountered in the viable epidermis.

Lesional AD skin shows less localized active GCase and ASM compared to control skin.

Lesional skin sections from three subjects were available for analysis. We first noted more keratinocyte layers in the viable epidermis compared to the control skin sections (supplemental figure S2). Moreover, in the lesional skin of patient #15 the SC appeared thicker and at some sections, corneocytes appeared swollen (supplemental figure S2). The expression of GCase at lesional skin sites was examined (figure 3, bottom panel). In patient #15 the expression of GCase was very similar to that in the control skin. In patient #13, GCase expression was sometimes observed at the SG/SC-interface, but mostly in the outermost keratinocyte layer in the viable epidermis close to the SG/SC-interface. Concerning patient #14, no GCase expression was detected at the lesional site, instead a diffuse signal was present in the whole viable epidermis. Additionally, in this patient nuclear expression was observed. When focusing on active GCase, in general this was localized in the SC matrix. In some parts of the sections of subject #13, no active GCase could be detected. However, in the majority of the cases of areas where activity was observed, a distribution throughout all the SC layers was observed. In skin sections of the other two patients active GCase was observed in the SC matrix, but mainly in the middle and outer layers of the SC and not in the lower layers of the SC.

ASM expression was not detected in patient #15, whereas the lesional sites of the other two subjects demonstrated expression at locations similar to that observed in the control skin sections. As far as active ASM is concerned, all lesional sections throughout all the SC lipid layers demonstrated activity. In the case of patient #14 the distribution throughout the SC was more scattered compared to the more evenly spread localization observed in the other two AD patients. Because the signal of ASM activity was throughout the whole SC of subject #15, the swollen corneoctes at the lesional sites of the SC were even more apparent.

Non-lesional AD skin demonstrates a high variety in localization of active enzymes.

A large variation was observed between the different subjects for GCase and ASM of non-lesional AD skin: localization patterns of active GCase and ASM varied between very comparable to control skin and similar to a lesional appearance. All the sections showed a GCase and ASM expression pattern similar to the control subjects, with two exceptions: i) Patient #9 showed additionally intra nuclear GCase expression; ii) non-lesional skin sections of patient #15 showed no ASM expression signal. The localization of active GCase was observed throughout the whole SC or in the lower layers of the SC, as described above for the control subjects. However, the localization in patient #7 was sometimes absent in the lower layers of the SC, corresponding with a more lesional distribution pattern. Active ASM localization was confined throughout the whole SC, either in a smooth or in a scattered pattern. Only patient #14 demonstrated no active ASM signal.

When combining all these findings we observe that the localization of active enzyme appeared more variable than the location of expressed enzyme. In general, active GCase and ASM are less localized near the SG/SC-interface in lesional and some non-lesional AD skin regions. As these changes in localization of enzyme activity may affect the SC ceramide composition, we thoroughly analyzed the SC lipids for each subject.

Increase in [AS] and [NS] ceramides relate with enzyme phenotype and disease severity.

We quantified the SC ceramides for each specific subclass and chain length Additional data on specific ceramides or glucosylceramides is listed in supplemental Figure S3 and supplemental Tables 2, 3 and Figure 4A demonstrates that AD patients have less absolute amount of total ceramides, particularly at lesional skin sites. Ceramide [NP] and [NH] were mostly reduced, as well as the EO ceramides. In contrast, ceramides [NS] and [AS] increased in absolute (and relative) amount in AD. Close examination revealed that the increase in these subclasses was dominated by ceramides with a very short chain length being 34 carbon atoms in total chain length, the so called C34 ceramides (Figure 4B and supplemental figure S4). We then related the amount of ceramides [AS]+[NS] to the different categories of activity patterns observed for ASM as described above (Figure 4C). The absence of clear ASM activity or clear localization near the viable epidermis and SG/SC-interface coincided with a relatively low [AS] and [NS] amount. In addition, subjects that had a more dispersed ASM activity localization compared to control subjects, demonstrated the most deviating amount of ceramides [AS] and [NS]. Thus, less localized active ASM around the SG/SC-interface correlates with an increased (and more varying) amount of [AS] and [NS]. We also observed the amount of ceramides [AS] and [NS] coinciding with an increase in local disease

severity (Figure 4D). Furthermore, a correlation was observed for active GCase and the ceramides that are synthesized by this enzyme only (all ceramides minus [AS] and [NS]), as is depicted in figure 4E. Absence of GCase activity near the SG/SC-interface results in a reduced amount of ceramides synthesized by GCase. Therefore, active GCase near the SG/SC-interface is crucial for a normal amount of ceramides synthesized by that enzyme.

The increase in short chain length ceramides and decrease in very long EO ceramides reduces the mean ceramide chain length in patients with AD, especially in lesional skin [18]. As the changes in ceramide chain length may be related to an impaired fatty acid elongation process [41], we quantified the FFA composition as well (Figure 4F). The calculated molar ratio *ceramides* : *FFAs* was 0.61±0.18 in the control group, 0.59±0.13 in non-lesional AD and 1.06±0.66 in lesional AD skin. Note that we excluded the short chain FFAs due to notorious contamination of C16:0 and C18:0, even nowadays in ultra-pure organic

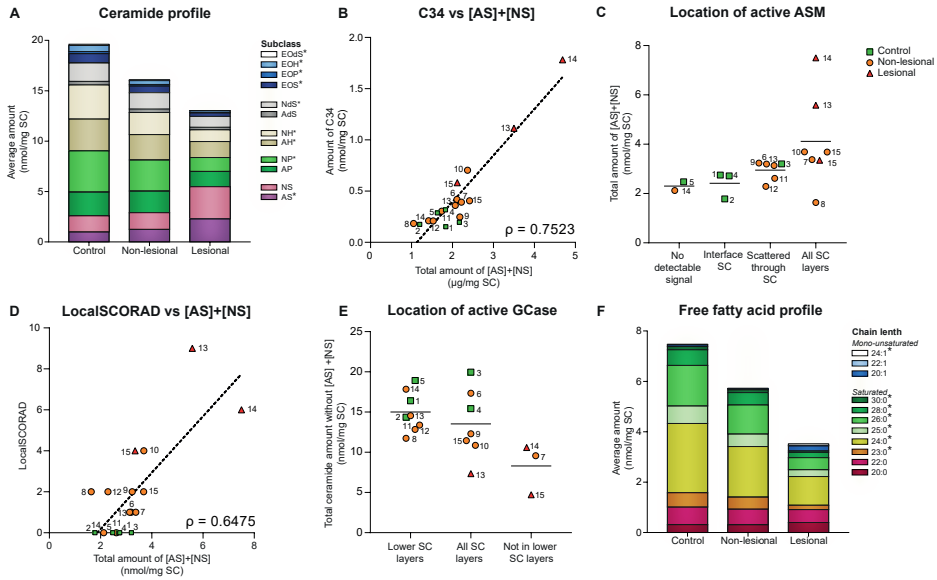

Figure 4: SC lipid data in control, non-lesional and lesional AD skin. A. Bar plots of average amount of ceramide subclasses in the SC. B. Dot plot amount of C34 ceramides plotted versus the total amount of [AS]+[NS] ceramides. C. Dot plot total amount of [AS]+[NS] ceramides plotted against the location of active ASM in the skin. D. Dot plot LocalSCORAD plotted against the total amount of [AS]+[NS] ceramides, E. Dot plot total amount of SC ceramides without¬ [AS]+[NS] compared to the location of active GCase location in the skin. F. Bar plots of average amount of SC FFAs categorized by length and degree of unsaturation. Significant ordinal trends (Jonckheere-Terpstra tests) for the ceramide and FFA quantities in A and F, respectively are shown for each lipid with a * ($p<0.05$). Horizontal lines in C and E represent means, and ρ-values in B and D depict Spearman correlations.

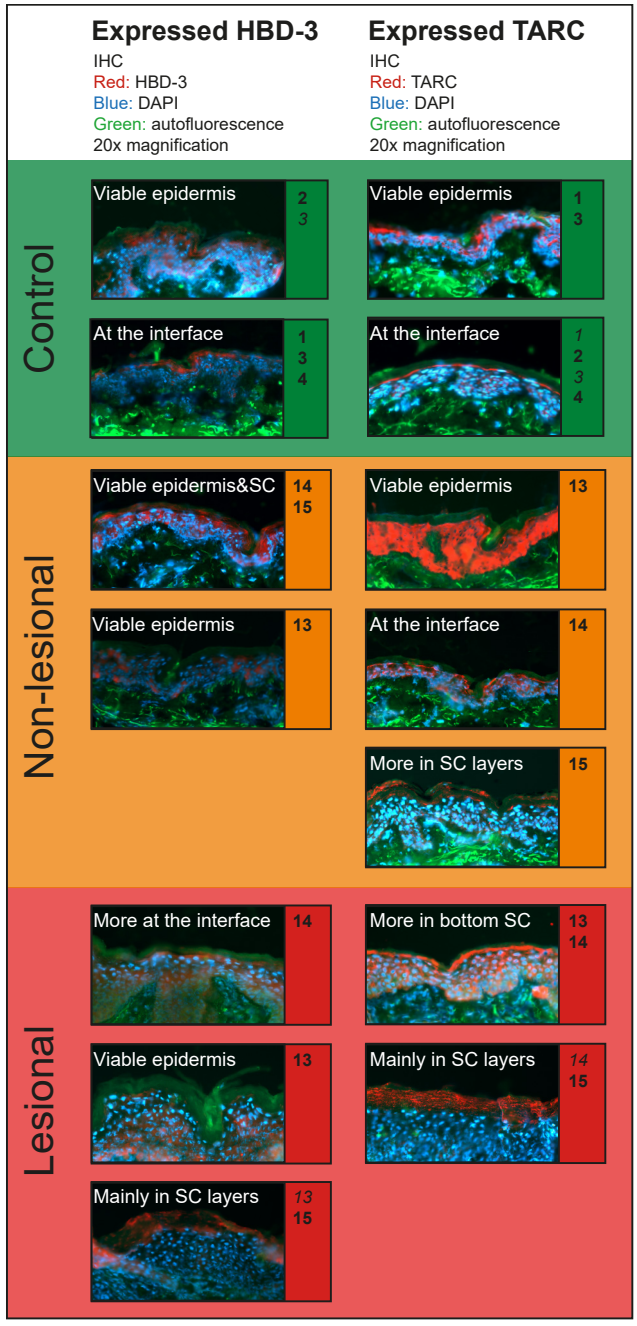

Figure 5: *In situ* localization of HBD-3 and TARC within skin sections of control, non-lesional AD and lesional AD skin. Microscopy images of skin sections showing in which skin layers HBD-3 and TARC are localized. Depicted are which localization patterns can be found in each subject. Bold numbers show its main occurrence per subject. Italic numbers demonstrate which patterns also appear in subjects, but are not the main pattern found in that individual.

solvents. This explains the difference in ratio-outcomes when comparing them to literature values [42, 43]. We observed also a decrease in absolute amount of FFAs in AD skin, particularly for ceramides with chain length of 23 carbon atoms or higher. This could be an indication for a relation between the decrease in FFA chain length to the increase in short chain ceramides belonging to the [AS] and [NS] subclass.

TARC and HBD-3 are less localized around the SG/SC-interface in lesional AD skin sections.

Besides the lipid enzymes, we also studied whether key inflammation markers (for AD) were changed systemically and locally. Systemically, we studied levels of TARC, Interleukin-22 and soluble IL-2 receptorin plasma, but no difference in these parameters between control and AD subjects was observed in this study cohort (data not shown).

In the skin the localization of TARC and HBD-3 were studied as a readout for inflammation and skin microbiome respectively. This is shown in Figure 5, for the control subjects and AD patients #13, #14 and #15 non-lesional and lesioanl regions. HBD-3 is mainly localized in the viable epidermis and occasionally slightly more confined around the SG/SC-interface in most control and non-lesional skin sections. There are non-lesional and lesional skin sections where HBD-3 is also present in the SC (non-lesional of subjects #14 and #15, lesional skin of subject #13). And in one patient, at the lesional site HBD-3 was more profound in the SC layers (#15).

Concerning the localization of AD marker TARC, its presence was generally in the viable epidermis and localized around the SG/SC-interface in control and non-lesional skin sections. In the lesional and some non-lesional skin sites, the expression of TARC was more abundant in the SC, either mainly in the bottom layers (non lesional section of #15 and lesional sites of #11 and #12) or throughout the whole SC (lesional skin section #15). Thus, delocalization of TARC was mainly detected in (inflamed) lesional AD skin as was observed with the active enzymes GCase and ASM.

Discussion

This study is the first that determines in one cohort of AD patients altogether the location of expressed and active SC lipid enzymes, and additionally relates this to a fully quantified SC ceramide and FFA composition. Here we demonstrate AD patients have an altered localization of GCase and ASM, particularly at lesional skin sites. The changes observed in (active) enzyme localization relate to altered ceramide levels and the ceramide subclass profile. These changes in SC lipids correlated with a disturbed skin barrier and

increased local disease severity.

Although our study cohort is small, it has identical clinical characteristics as comparable studies reported previously (i.e. TEWL, SCORAD, SC, skin barrier lipid properties) [17-19, 28, 44, 45]: i) On a general level, AD patients demonstrate a decrease in amount of SC lipids (both ceramides and FFAs), which is more substantial at lesional skin sites. ii) When observing the SC lipids in more detail, a shift towards shorter ceramides and FFAs is seen in AD patients. iii) An increase in subclasses that are particularly related to ASM ([AS] and [NS]) was observed at the expense of ceramide [NP] and [NH], a feature of AD that is observed in almost every AD cohort.

When correlating the SC lipid composition to the enzyme expression/activity, one should realize that there is a time-aspect difference between both parameters: The ceramide composition is the result of an accumulation of the lipid synthesis products for at least 20 days prior to the study day, whereas the biopsies and *in situ* expression/activity images are visualizations at a specific time point – the study day itself. Nevertheless, despite this time-issue and the small sample-size of our cohort, we were able to establish clear changes in the lipid enzymes and correlate these to the SC ceramide phenotype.

A previous study has shown reduced ASM activity in non-lesional and lesional AD epidermis compared to controls, while proposing reduced sphingomyelin levels were not caused by the downregulated ASM levels [26]. In addition normal GCase activity in AD SC has been reported [25]. The present study is the first to study in which both, active GCase and ASM were localized throughout the whole epidermis and related to changes observed in SC ceramide subclass profile in AD. More specifically, we demonstrate that the location of active enzyme rather than the location of expressed enzyme correlates with AD disease manifestation. This elucidates why previously no correlations between enzymes and SC lipids were observed [28], as detailed localization of active GCase and ASM has never been described in AD. Due to the recent development of visualization techniques by ABP-labeling and *in situ* zymography for GCase and ASM [46, 47], their localization can now be studied in detail. Besides to the aforementioned changes in localization of active GCase and ASM in AD, we also observed, on a micro-level scale, a high variation in location of active GCase and ASM. Lipid content over depth has previously been shown to be homogeneous [48]. However, because local changes are observed for the (active) enzymes GCase and ASM, local differences in lipid composition cannot be excluded. No techniques with sufficient resolution are available yet to measure these changes in lipid compositions locally. The underlying reason for high variation in the location of active enzyme is unknown, but literature mentions changes in the micro-environment as one of the most plausible reasons [29]. Changes in micro-environment may affect the local distribution of microflora (which relates to our local changes in antimicrobial peptide

HBD-3 expression), and also the local acidic environment (so-called skin-pH). Literature reports slightly elevated levels in skin-pH in AD [38], even in non-lesional skin [49]. This change in skin-pH could affect the activity of GCase and ASM *in vivo*, as the optimal pH value for GCase and ASM are respectively 4.5 and 5.6 [50]. In addition, we analyzed the skin-pH, but did not observe substantial differences between healthy subjects and AD-patients. However, if these environmental changes in acidity vary to a high extent on a micro-scale, this would align with the micro-scale localization differences in active GCase and ASM. Another important factor for optimal enzyme activity is the presence of cofactors. Saposin C is necessary for proper GCase activity, and dysfunction in this cofactor could lead to insufficient ceramide conversion, as is the case in specific Gaucher cohorts [51]. The role of saposin C in relation to AD is unknown, but it has been reported that protein amount of precursor prosaposin is decreased in AD [52] which could hamper proper functioning of GCase.

GCase converts glucosylceramides into the final SC barrier ceramides. Previously no difference in GCase activity between lesional and control skin was found [25]. However, we observed that active GCase is less localized around the SG/SC-interface and lower SC layers in lesional AD skin compared to control. This is in line with previous observations by Holleran et al., who demonstrated changes in localization of GCase activity (relative increase in upper parts of the epidermis) in mice with a skin barrier disruption [53]. In our study, the altered location of active GCase correlates with a decreased amount of overall SC ceramide levels, particularly the subclasses that cannot be synthesized by ASM. This corresponds with the localization of active ASM being present in additional (more outer) SC layers besides being mainly localized at the SG/SC-interface, as observed in the control group. The increase of ceramides [AS] and [NS] correlated to clinically relevant parameters for skin barrier function (TEWL) and disease severity (SCORAD). Other reported studies in different cohorts and skin diseases that found comparable changes in ceramides [AS] and [NS] (reviewed by [19]), implies that the by ASM derived [AS] and [NS] ceramides are involved in circumstances relate to stressed/diseased skin. This could indicate ASM has a different function than GCase in the skin, as they also have different roles in other organs and tissues: GCase is a key lysosomal enzyme, responsible for main physiological functions of almost every cell, and a key enzyme in glucosylceramide metabolism under healthy/physiological conditions and is considered a housekeeping enzyme [54]. On the contrary, ASM is usually referred as a mediator in pathological processes like cell stress and apoptosis [55]. A switch from physiological conditions towards pathophysiological conditions, like observed here between healthy and AD, may imply that these enzymes have comparable (patho)physiological roles in the skin as they have elsewhere in the human body. Besides, the localization

of expressed TARC, a chemokine triggered in inflammatory diseases like AD, is also changed in AD subjects and could be observed throughout the SC rather than only in the viable epidermis or at the SG/SC-interface [56, 57]. Note that these AD subjects did also demonstrate active ASM throughout the SC.

Literature reports TARC as one of the most significant biomarkers to date for diagnosing AD [58]. We did not observe a correlation between the localization of TARC in the skin and systemic TARC analyzed from plasma. However, visualizing this expressed biomarker in the epidermis does already demonstrate local changes, that might not be visible systemic yet. This all indicates that for interpreting local changes in AD severity, visualization of the local epidermal environment may facilitate in elucidating differences between clinical appearance of AD patients.

The reduction we found in [NP] ceramides (and increase in [AS] and [NS]), can also – at least partially – be explained by changes in dihydroceramide desaturase enzymes (DEGS1 and DEGS2), involved in the conversion of [dS]-ceramides into respectively [S]-ceramides and [P]-ceramides. An increase in expression/activity of DEGS1 relative to DEGS2 would increase the amount of [S] ceramides at the expense of [P] ceramides. The analysis of DEGS-enzymes is beyond the scope of this manuscript, and currently no methods are available for visualizing *in situ* DEGS activity.

We have shown the importance of correct localization of SC enzymes and how this correlates with previously published characteristics of AD, as well as SC lipid composition. We demonstrated changes in SC lipid composition directly affect the skin barrier function (and indirectly disease severity). As these changes originate (at least partially) from changes in the activity of the enzymes, a possible new target for therapy would be to restore the activity of GCase and ASM in AD skin to that of control skin, thereby aiming for repairing the ceramide composition in AD.

Acknowledgements

We thank Walter Boiten for his valuable input regarding the analysis of the ceramide data.

Materials and Methods

Subject inclusion and skin sample processing. The study was conducted according to the Declaration of Helsinki principles. Caucasian AD patients and control volunteers of age 18-40 were included in the study and assessed using SCORAD (SCORing Atopic Dermatitis) [40] and EASI (Eczema Area and Severity Index) [39]. A full overview of all exclusion criteria is provided in supplemental materials and methods. Individuals had a 4-week washout period during which it was not allowed to use soaps or cosmetics on the ventral forearms. Subjects with lesional AD skin were put on standard medication that did not contain any interfering lipids (see 'Use of standardized formulations' in the supplement). After 4 weeks the participants were scored again for SCORAD and EASI. This was followed by monitoring skin-pH and TEWL in depth after SC removal by tape stripping from a marked area on their ventral forearm. TEWL was measured with a closed chamber evaporimeter (Aqua Flux AF200: Biox Systems Ltd, London, UK) and skin-pH was measured with a skin-pH Portable Meter - HI99181 – (Hanna Instruments, Nieuwegein, NL). Subsequently two 4 mm punch biopsies were collected from the non-lesional AD skin and skin from controls, adjacent to the tape stripped sites. Two additional biopsies were obtained from three AD patients that had lesional skin sites on their ventral forearms. Biopsies were used either for SC lipid analysis or were snap frozen with matrix specimen Tissue-Tek (Sakura Finetek, Alphen a/d Rijn, Netherlands) in liquid nitrogen. Frozen samples were cut to 5 µm thick sections (Leica CM3050s, Leica Microsystems, Germany), placed on SuperFrost plus microscope slides (VWR International, Netherlands) and stored at -80°C prior to being used for enzyme studies.

SC lipid isolation and analysis. The SC of one of the biopsies was isolated by a common trypsin digestion procedure [59], followed by SC lipid isolation with use of an extended Bligh and Dyer extraction [60, 61]. The SC lipids were reconstituted in heptane:chloroform:methanol (95:2.5:2.5) and the exact ceramide and FFA composition was finally determined by liquid chromatography/mass spectrometry (LC/MS), as previously reported [61]. Briefly, a normal phase pva-column (100 x 2.1mm i.d., 5µm particle size; YMC Kyota, Japan) attached to and Acquity UPLC H-class device (Waters, Milford, MA, USA), programmed with an elution gradient of heptane toward heptane:isopropanol:ethanol (50:25:25), was used to separate the ceramides subclasses by chromatography. A Waters Xevo TQ-S MS, equipped with an atmospheric pressure chemical ionization (APCI) source was used for all mass analysis in positive ion full scan mode of the lipids. Data presented in absolute amounts (nmol/µg SC) was obtained by applying our reported quantitative model by using deuterated internal standards (Ceramides EOS and NS).

For FFA analysis, a new method was developed based on our previously

reported analysis [62]. A Purospher Star LiChroCART column (55x2 mm i.d., 3 µm particle size; Merck, Darmstadt, Germany) was used to separate FFAs while a solvent gradient of acetonitrile:H2O (90:10) to methanol:heptane (90:10) was maintained at 0.5 mL/min. For ionization optimization, addition of 2% chloroform and 0.005% acetic acid led to stable [M+Cl]- and [M-H]- traces, both analyzed in SIR negative ion mode using a Waters XEVO TQ-S MS with an IonSabre APCI MkII probe. Details of this method are provided in the supplement.

Statistics. Statistical tests were performed using Graphpad Prism v6 (GraphPad Software, La Jolla California USA) and IBM SPSS Statistics v24 (IBM, New York, NY). Most data appeared non-normally distributed, hence we used non-parametric statistics: significant ordinal trends in the SC lipid quantities (ceramides and FFAs) were determined using the Jonckheere-Terpstra trend tests. Spearman's ρ were calculated to indicate correlation coefficients. Significance was set at the $p<0.05$ level.

Immunohistochemical staining of ASM, GCase, HBD-3 and TARC. Skin cryosections were washed three times with PBS and blocked in PBS containing 1% (v/v) BSA and 2.5% (v/v) horse serum. Next, sections were incubated overnight at 4°C with any of the primary antibodies diluted in 1% BSA in PBS. Thereafter, sections were washed with PBS and labeled for one hour at room temperature with secondary antibody diluted in 1% BSA in PBS. Then sections were washed twice in PBS, once in demi-H2O and finally mounted with Vectashield with diamidino-phenylindole solution (DAPI, Vector Laboratories, Burlingame, CA). Antibody details and dilution factors are depicted in table 1.

In-situ *ABP labeling GCase.* Active GCase was visualized by labeling with the ABP MDW941 as we reported previously [63]. Briefly, skin cryosections were washed in MilliQ with 1% (v/v) Tween-20 (Bio-Rad Laboratories), followed by

Table 1: Overview primary and secondary antibodies.

	Antibody	Dilution ratio	Binding	Antibody brand
1st	Anti-GCase	1:150	Human anti rabbit	Abcam (ab125065)
	Anti-ASM	1:150	Human anti mouse	Novus (NBP2-45889)
	Anti-HBD-3	1:1500	Human anti rabbit	Abcam (ab19270)
	Anti-TARC	1:100	Human/rat/mouse anti rabbit	Abcam (ab182793)
2nd	Rhodamine red	1:300	Goat anti rabbit	Jackson ImmunoResearch (711-295-152)
	Cy3	1:1000	Goat anti mouse	Abcam (ab97035)

incubation with 100nM of MDW941 in McIlvain buffer (150 mM citric acid-Na2HPO4 (pH 5.2)) with 0.2% (w/v) sodium taurocholate and 0.1% (v/v) Triton X-100 for 1 hour at 37°C. Then samples were washed once with MilliQ with 1% (v/v) Tween-20 and afterwards three times with MilliQ water. Mounting was performed using Vectashield with DAPI solution.

In-situ *zymography ASM.* Active ASM was visualized by our recently developed *in situ* zymography method using 6-HMU-PC (Moscerdam, Oegstgeest, the Netherlands) as ASM specific substrate [47]. Skin samples were washed in MilliQ with 1% (v/v) Tween-20. The sections were incubated in 0.1M sodium acetate buffer pH5.2 containing 0.5mM 6-HMU-PC in, 0.02% (w/v) sodium azide and 0.2% (w/v) sodium taurocholate at 37°C for one hour. Subsequently, samples were dip-washed twice with MilliQ with 1% (v/v) Tween-20. Mounting was performed using Vectashield with Propidium iodide (PI, Vector Laboratories, Burlingame, CA).

Fluorescence microscopy. Microscopy images were taken with a Zeiss Imager. D2 microscope connected to a ZeissCam MRm camera (Zeiss, Göttingen, Germany) with objective magnification 10x and lens magnification between 10-63x (with immersion oil). Zen 2 2012, blue edition (Zeiss) was used for image processing. Exposure times were kept constant for each individual experiment. Gamma was set to 1.0 for all measurements. Enzyme activity was determined at its optimal magnification 63x. Activity of ASM was visualized by 6-HMU at λex=380 nm and λem=460 nm, whereas active GCase was visualized with ABP MDW941 at λex=549nm, λem=610nm. Microscopy images were independently scored by two researchers on the location of GCase, ASM, HBD-3 and TARC.

Supplemental Materials and Methods

Exclusion criteria for participation in the study. A potential subject who met any of the following criteria was excluded from participation in this study:

Exclusion criteria for healthy subjects and AE patients

- Aged under 18 or over 40.
- Non-Caucasian.
- Abundant hair presence on the ventral forearms.
- Unnatural abnormalities on one of their ventral forearms (e.g. skin lesions, tattoos).
- Using any systemic drug therapy (e.g. cholesterol-lowering drugs, insulin related drugs, steroids and immunosuppressants).
- Who received phototherapy in the past 2 years.
- Pregnancy.

Additional exclusion criteria for healthy subjects:
- No chronically inflammatory disease.
- Use of dermatological products (e.g. creams) on their ventral forearms on a daily basis.
- Dermatological disorders or a history of dermatological disorders.

Additional exclusion criteria for AE patients:
- The absence of both lesional and non-lesional skin sites on their ventral forearms at day 0 of the study. Thus, when patients only have non-lesional skin sites at their ventral forearms of Day 0, but not inflamed, red lesions, they will be excluded as one of the key objectives is to investigate within the same subject non-lesional skin with lesional skin.
- The use of corticosteroids class IV or higher. Patients with corticosteroids class I-III need to give informed consent about changing their medication to a standardized regimen (see "3) study design").

Besides, all subjects were requested:
- Not to change their usual skin care regimen (except for topical corticosteroids, as described above).
- The forearms should not be exposed to excessive sun- or artificial UV-light.
- Not to smoke or start smoking 3 weeks prior or during the experiment;
- Not to drink warm and/or caffeine containing beverages on the day of the experiment.
- Not to apply any topical formulation on their ventral forearms on day 28 (study day).
- To leave the application site(s) untouched during the day of the experiment.
- To keep an agenda for 3 weeks in advance in which they describe and take photographs of their ventral forearms once every day. In this way, we have more information about the history of the lesional skin prior to the primary investigation day.

Use of standardized formulations. Patients with atopic eczema often do apply topical formulations of any kind on their body. This includes sometimes class 1-4 corticosteroids. These formulations highly influence with the primary analysis and objectives:
1) Many topical formulations and emollients contain lipids that are also present in human skin. This highly interferes with our lipid composition data.
2) Corticosteroids have a systemic effect on the inflammation, thereby significantly altering the inflammation markers locally and systemically.

Stardardized treatment during the study period was therefore as follows:
- Patients that did not apply any topical continue this until day 28.
- Patients that applied non-corticosteroid formulation switched to a cetomacrochol cream.
- Patients that applied class 1 corticosteroids switched to a 0.1% hydrocortisone

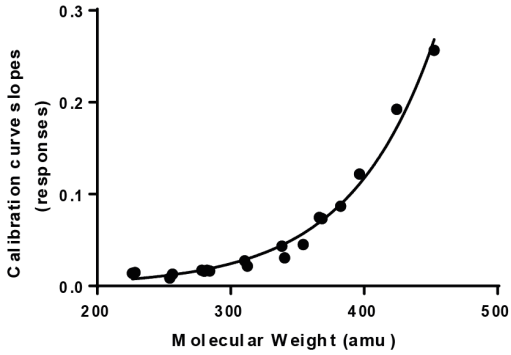

acetate in cetomacrochol cream with emollient cetomacrochol.
- Patients that applied class 2 or 3 corticosteroids switched to 0.1% triamcinolon acetonide in cetomacrochol with emollient cetomacrochol.
- Patients that applied class 4 corticosteroids were excluded from the study.

Analysis of Stratum Corneum fatty acid composition by LC/MS. Isolated Stratum Corneum fatty acids from biopsies of all AD patients and controls were quantitatively analyzed by ultra performance liquid chromatography/mass spectrometry (UPLC/MS), adapted from our previously reported analysis (van Smeden et al., BBA, 2014). Tables I, II, and III below provide all detailed

Table I: UPLC setup

UPLC system	Waters Acquity UPLC H-Class
UPLC reverse phase C18	Purospher Star LiChroCART (55x2 mm, 3µm)
UPLC reverse phase C18	
- Heating tray temperature	- +40°C
- Wash solvent	- MeOH:Heptane:IPA (25:50:25%)
- Injection volume	- 10µl
Mobile Phase	
- Flow rate	- 0.5 mL/min
- Solvents	
- Acetonitrile	- ULC/MS grade, Biosolve (012041)
- Methanol	- ULC/MS grade, Biosolve (136841)
- Heptane	- ULC/MS grade, Boom (76025346.2500)
- Ionization enhancers/stabilizers	
- Chloroform (2%)	- HPLC grade, Labscan (C07C11X)
- Acetic acid (0.005%)	- HPLC grade, Biosolve (01070601)

information on parameters for respectively LC, MS, and validation parameters of the quantified analytes.
Absolute quantification was achieved taking into account the different response factors for each ion trace (see Figure on the right). The individual response factors were obtained via analysis of calibrators (see table III) in addition to an internal standard (ISTD) correction using deuterated ISTDs C18:0 D35 and C24:0 D47. Mass Lynx and Target Lynx Software (Waters) was used to process the data.

Table II: MS setup.

MS System	MS System
LC/MS interface	LC/MS interface
- Probe	- Probe
- Corona discharge current	- Corona discharge current
- Cone voltage	- Cone voltage
- APCI probe temperature	- APCI probe temperature
- Desolvation gas volume	- Desolvation gas volume
- Cone gas volume	- Cone gas volume
Scan Method	Scan Method
- Ionization mode	- Ionization mode
Scan settings/trace	Scan settings/trace
- Scan time	- Scan time
- Inter scan Delay	- Inter scan Delay
- Collision gas flow (Q2)	- Collision gas flow (Q2)
- Collision Voltage (Q2)	- Collision Voltage (Q2)
MS Resolution	MS Resolution
- Q1	- Q1
- Q3	- Q3

Table III: Validation parameters.

	Fatty acid (length : saturation)	Ion trace(s)* (amu)	Rt (min. ± SD)	Calibration curves (R-value)**
Saturated Fatty Acids	20:0	311.46 + 347.37	2.23 ± 0.012	0.993
	22:0	339.37 + 375.35	2.68 ± 0.008	0.995
	23:0	353.36 + 389.33	2.87 ± 0.005	0.998
	24:0	367.41 + 403.38	3.03 ± 0.022	0.995
	25:0	381.46 + 417.37	3.16 ± 0.005	0.997
	26:0	395.51 + 431.42	3.29 ± 0.003	0.996
	28:0	423.48 + 459.46	3.55 ± 0.004	0.994
	30:0	451.52 + 487.43	3.83 ± 0.005	0.995
Unsaturated Fatty Acids	20:1	309.38 + 345.36	1.63 ± 0.024	0.991
	22:1	337.36 + 373.33	2.19 ± 0.004	0.996
	24:1	365.39 + 401.31	2.68 ± 0.049	0.995

*: Masses correspond to ions [M-H]- + [M+Cl]-. ** Correlation values of 3 independent calibration curves (range 1-100 pmol) with a mixture of 11 fatty acids and two deuterated internal standards.

Supplemental data

Supplemental table S1 - Disease manifestation and main location of the (active) enzymes per individual subject: The main localization pattern is mentioned first, italic depicts the less abundant pattern that sometimes is also found in the subject. Green = control; orange = non-lesional AD ; red = lesioanl AD.

Nr	Sex	TEWL	SCORAD day28	local SCORAD day 28	EASI day 28	Expressed GCase	Active GCase	Expressed ASM	Active ASM
1	F	12.44	0	0	0	At the interface	Lower layers SC *Whole SC*	Viable epidermis	Around interface *Scattered through SC*
2	M	8.81	0	0	0	At the interface	Lower layers SC	Viable epidermis	Around interface
3	F	11.65	0	0	0	At the interface	Whole SC	Viable epidermis	Scattered through SC *Around interface*
4	F	10.32	0	0	0	At the interface	Whole SC *Lower layers SC*	Viable epidermis	Around interface
5	F	7.92	0	0	0	At the interface	Lower layers SC *Whole SC*	Viable epidermis	No detectable signal
6	M	12.83	15.4	1	3.2	At the interface	Whole SC	Viable epidermis	Scattered through SC *Whole SC*
7	F	19.19	18.2	1	1.8	At the interface	Not in lower SC layers *Whole SC*	Viable epidermis	Whole SC
8	F	8.37	23	2	1	At the interface	Bottom SC layers	Viable epidermis	Whole SC *Scattered through SC*
9	F	11.34	13.9	2	5	At the interface	Whole SC *Bottom SC layers*	Viable epidermis	Scattered through SC

Continuation supplemental table S1 - Disease manifestation and main location of the (active) enzymes per individual subject: The main localization pattern is mentioned first, italic depicts the less abundant pattern that sometimes is also found in the subject. Green = control; orange = non-lesional AD ; red = lesioanl AD.

Nr	Sex	TEWL	SCORAD day28	local SCORAD day 28	EASI day 28	Expressed GCase	Active GCase	Expressed ASM	Active ASM
10	M	25.3	41.16	4	5.7	At the interface	Whole SC	Viable epidermis	Whole SC
11	F	14.99	8.8	0	0.3	At the interface	Bottom SC layers *Whole SC*	Viable epidermis	Scattered through SC
12	M	17.94	22.6	2	1.4	At the interface	Bottom SC layers	Viable epidermis	Scattered through SC
13	M	8.39	64.3	1	29.8	Below interface *At the interface*	Bottom SC layers *Whole SC*	Viable epidermis	Scattered through SC
13	M	24.46	64.3	9	29.8	At the interface	Whole SC *No detectable signal*	Viable epidermis	Whole SC
14	F	5.03	20.1	0	1.2	Not at the interface	Bottom SC layers *Whole SC*	Viable epidermis	No detectable signal
14	F	38.51	20.1	6	1.2	At the interface	Not in lower SC layers	Viable epidermis	Scattered through SC *Whole SC*
15	M	23.74	31.1	2	4.9	At the interface	Whole SC	No detectable signal	Whole SC
15	M	22.36	31.1	4	4.9	At the interface	Not in lower SC layers	No detectable signal	Whole SC

Supplemental table S2 – Ceramide class data per individual subject.: Green = control; orange = non-lesional AD ; red = lesioanl AD.

Code	NdS	NS	NP	NH	AdS	AS	AP	AH	EOdS	EOS	EOP	EOH
1	1587.3	1736.1	3831.7	3543.1	290.2	977.7	1918.5	3130.1	94.0	1103.0	184.9	724.2
2	1774.2	1076.3	3516.9	2595.4	374.8	709.4	2357.5	2639.4	88.6	536.4	128.3	350.3
3	1897.8	2020.1	4550.2	4308.3	372.2	1182.8	2427.2	3890.1	110.8	1300.2	231.5	870.9
4	1663.9	1452.4	3317.1	2424.2	396.8	1296.6	3114.9	3445.0	74.0	541.0	116.3	342.9
5	2257.2	1632.5	5242.4	3943.6	378.3	846.0	2023.9	2681.0	145.3	1113.9	311.9	827.0
6	2608.2	1823.0	4186.4	2669.9	573.7	1373.1	3008.3	3064.2	100.8	653.8	143.8	343.9
7	1014.5	1898.7	1587.9	1848.3	224.7	1475.6	1176.5	2392.2	82.1	778.3	80.0	389.9
8	1408.3	1085.0	2938.7	2486.0	224.3	548.6	1408.5	1952.8	97.4	644.5	138.4	443.5
9	1994.0	1733.8	2591.5	1622.8	439.2	1503.3	2458.6	2566.1	67.5	299.0	95.5	163.1
10	1371.9	1955.9	2273.7	1656.8	403.7	1736.8	2035.6	2212.4	55.4	501.9	105.8	255.5
11	1556.8	1562.6	2861.8	2538.1	324.4	1056.7	1757.0	2392.8	124.3	1082.6	175.3	568.3
12	1425.6	1371.0	3189.9	2214.0	259.1	921.9	2261.6	2502.1	66.6	501.3	130.0	301.3
13	1633.9	1664.2	3283.4	1930.9	390.7	1469.2	2931.1	3269.0	86.2	566.1	140.2	310.1
13	892.7	3082.5	1356.3	973.5	249.3	2500.5	1814.1	1593.1	23.3	278.4	54.7	118.5
14	1931.9	1410.4	5705.6	3383.0	306.1	713.7	1975.8	2321.0	109.0	1050.2	299.4	758.4
14	1774.6	4666.9	2034.8	1658.5	400.3	2834.0	1797.1	1986.3	44.3	582.3	95.7	229.5
15	1269.3	1968.3	2290.4	1540.6	287.5	1714.6	2512.3	2449.0	70.4	624.4	114.4	293.0
15	541.9	1798.5	772.1	814.0	146.1	1548.8	941.3	1176.1	11.5	187.5	32.3	92.3

Supplemental tables S3 – Semi-quantitative GlcCer data: Top: Average GlcCer/Cer ratio EOH subclass as mean +/- SEM. Bottom: Average GlcCer/Cer ratio EOS subclass as mean +/- SEM.

	EOH66	EOH67	EOH68	EOH69	EOH70
Control	0.09 ± 0.03	0.09 ± 0.03	0.09 ± 0.03	0.07 ± 0.03	0.06 ± 0.03
Non-lesional	0.18 ± 0.04	0.17 ± 0.04	0.16 ± 0.03	0.14 ± 0.04	0.13 ± 0.03
Lesional	0.28 ± 0.17	0.23 ± 0.13	0.22 ± 0.15	0.21 ± 0.14	0.18 ± 0.12

	EOS64	EOS66	EOS67	EOS68	EOS69	EOS70	EOS71	EOS72	EOS74
Control	0.13 ± 0.10	0.32 ± 0.11	0.28 ± 0.08	0.23 ± 0.07	0.19 ± 0.06	0.18 ± 0.04	0.18 ± 0.04	0.20 ± 0.05	0.14 ± 0.02
Non-lesional	0.37 ± 0.13	0.64 ± 0.14	0.51 ± 0.09	0.42 ± 0.08	0.32 ± 0.06	0.28 ± 0.05	0.26 ± 0.04	0.24 ± 0.04	0.18 ± 0.02
Lesional	0.32 ± 0.25	0.60 ± 0.31	0.50 ± 0.26	0.47 ± 0.22	0.54 ± 0.31	0.46 ± 0.22	0.80 ± 0.43	0.47 ± 0.20	0.23 ± 0.06

Supplemental figures

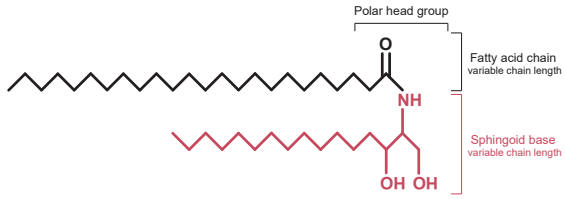

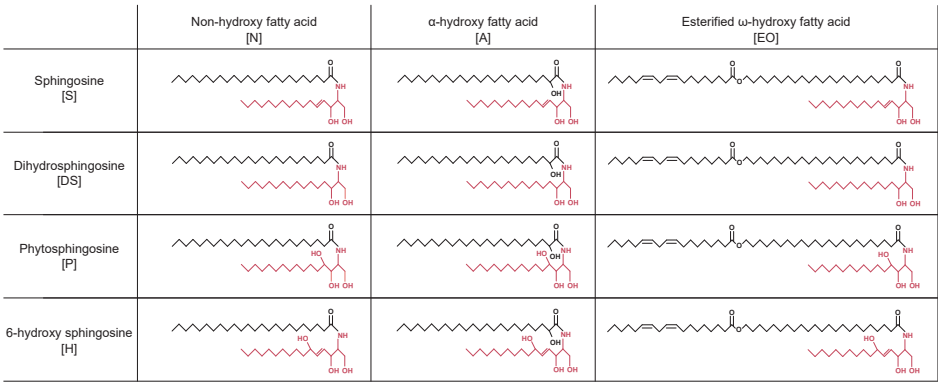

Supplemental figure S1: Table of the 12 common SC ceramide subclasses. Ceramide nomenclature including the molecular architecture. A ceramide is composed of a fatty acid chain (labeled in gray) linked via an amide bond to a sphingoid base (depicted in blue). In human skin, both chains vary in length (red arrows), leading to a total chain length (the two combined chains together) that varies from very short (~34 carbon atoms) to very long (>80 carbon atoms) chains. In addition, both chains can have additional functional groups at the carbon positions marked in red. This results in 4 different sphingoid bases (dihydrosphingosine [dS], sphingosine [S], phytosphingosine [P], 6-hydroxysphingosine [H]) and 3 different acyl chains (non-hydroxy fatty acid [N], α-hydroxy fatty acid [A] and the ultra-long esterified ω-hydroxy fattyacid [EO]). Together, this results in the presence of the 12 most common presented subclasses. As an example, a cer with a non-hydroxy fatty acid of 16 carbon atoms long and a sphingosine base of 18 carbon atoms will be denoted as ceramide [NS] C34.

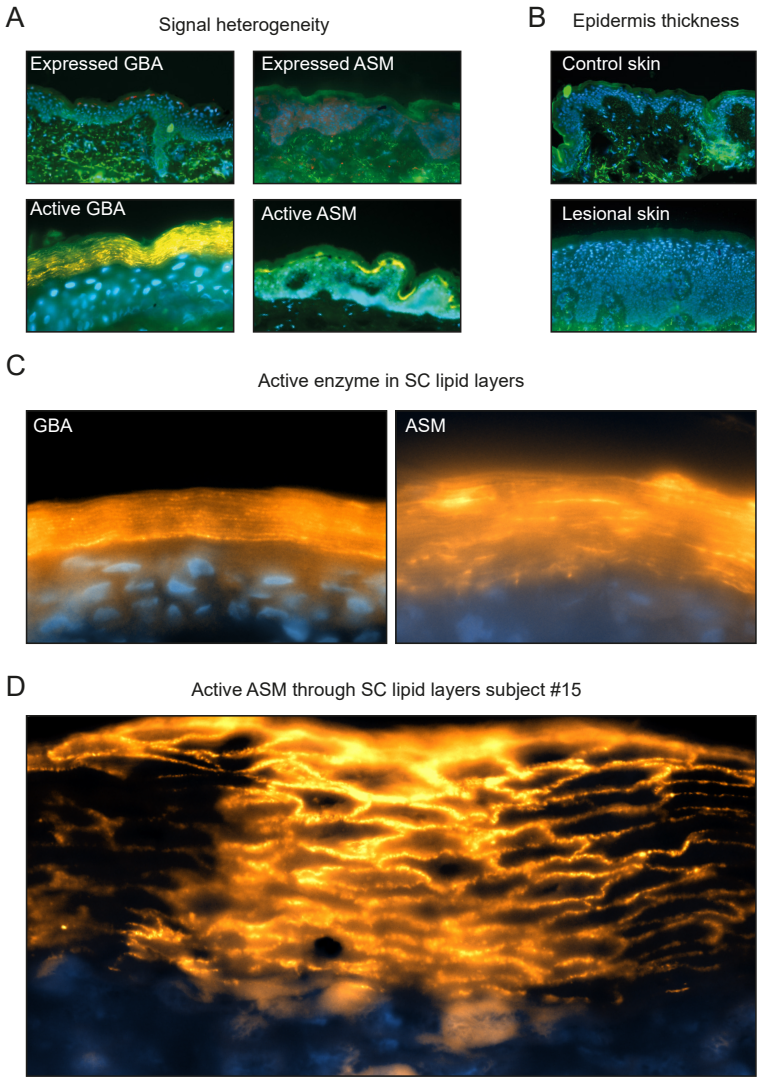

Supplemental figure S2: *In situ* heterogeneity localization GCase and ASM, lesional AD skin morphology and localization of active GCase and ASM in the SC lipid layers. A. Examples of heterogeneity of the fluorescence signal of expressed and active GCase and ASM. Left top: Expressed GCase (red) in subject #11. DAPI staining in blue and autofluorescence in green, 20x magnification. Left bottom: Active GCase (gold) in subject #7. DAPI staining in blue and autofluorescence in green, 63x magnification. Right top: expressed ASM (red) in subject #3. DAPI staining in blue and autofluorescence in green, 20x magnification. Right bottom: active ASM (gold) in subject #2. PI staining in blue and autofluorescence in green, 20x magnification. B. Epidermis in control skin (top) and in lesional skin (bottom). DAPI staining in blue and autofluorescence in green, 20x magnification. C. Active SC enzymes in the SC lipid layers. GCase (left, gold. DAPI in blue) in subject #1 and ASM(right, gold. PI in blue) in subject #10, 63x magnification. D. Example of swollen corneocytes in the SC of lesional skin of subject #15, active ASM in gold, PI in blue, 63x magnification.

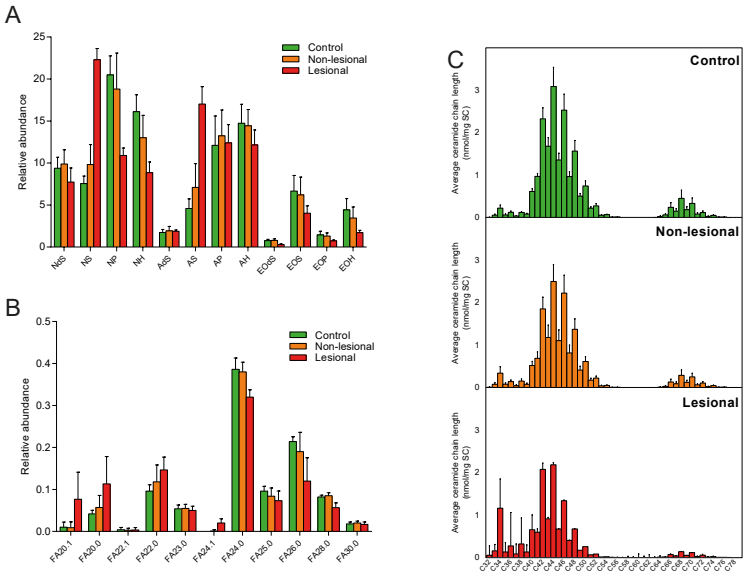

Supplemental figure S3: Lipid data SC. A. Bar plot of the relative amount of ceramides in the SC classified by category (mean ±SD). B. Bar plot of the relative amount of SC fatty acids categorized by length and saturation (mean ±SD). C. Bar plots of the abundances of the ceramide chain length subclasses per control, non-lesional and lesional group (mean±SD).

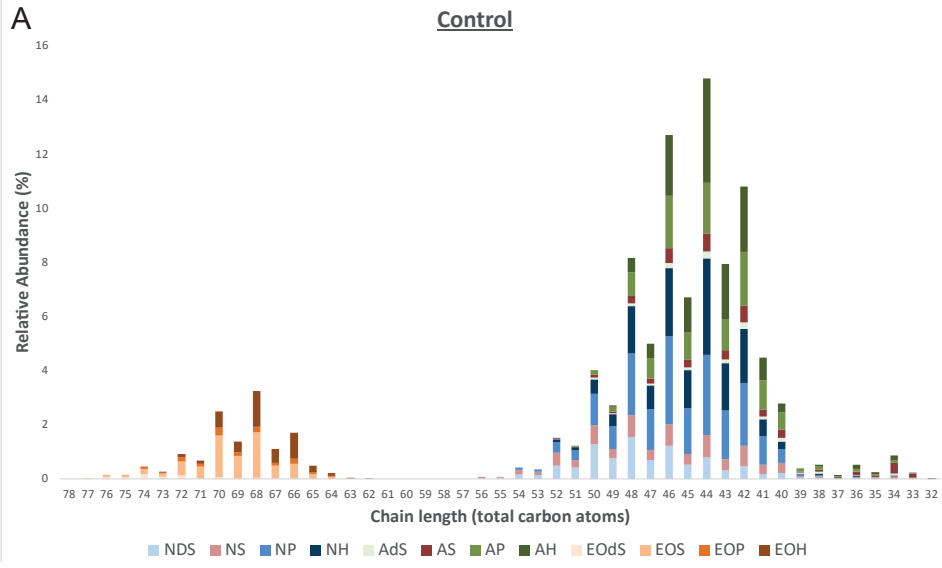

Supplemental Figure S4A: Bar plots of the relative abundances (%) of the ceramide chain lengths, labelled for each individual subclass, displayed for control

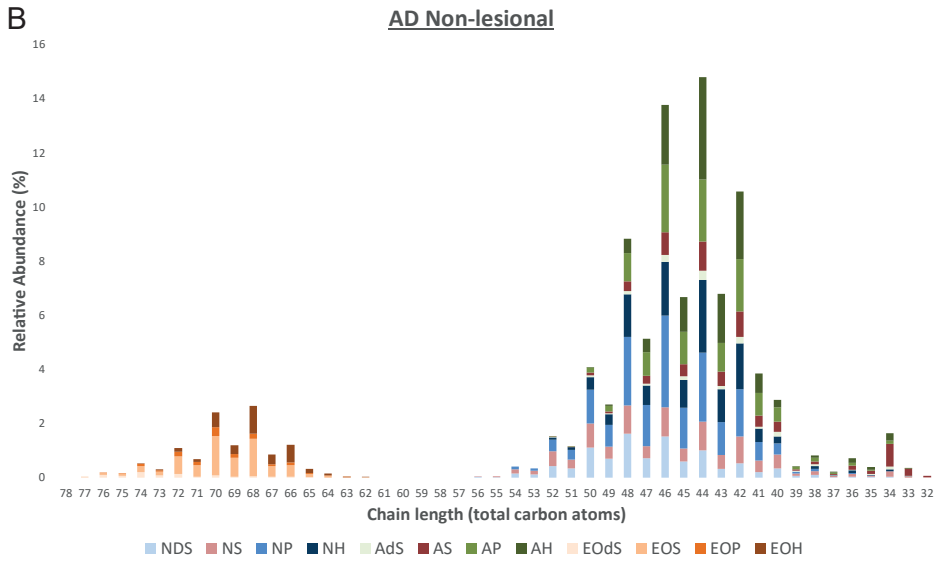

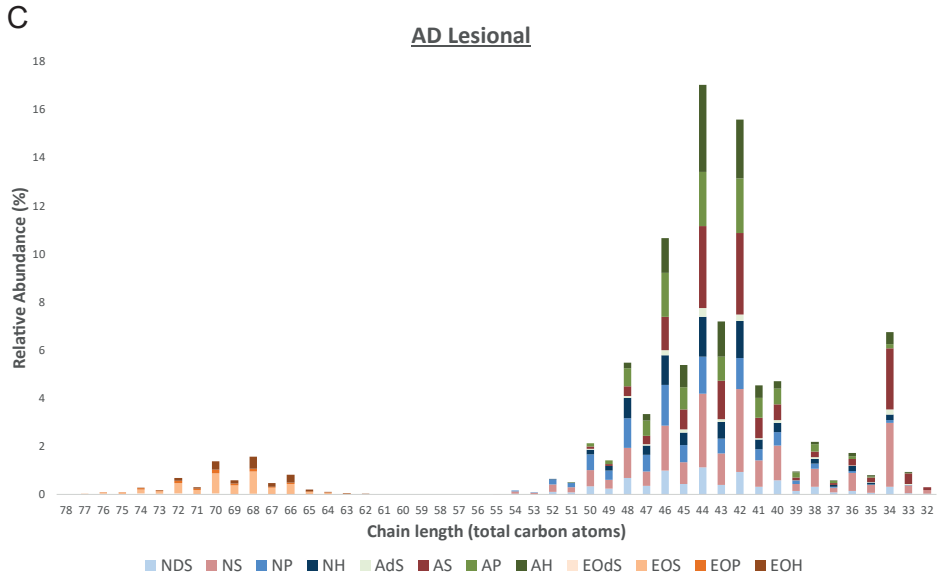

Supplemental Figure S4B and S4C: B. Bar plots of the relative abundances (%) of the ceramide chain lengths, labelled for each individual subclass, displayed for non-lesioanl AD. C. Bar plots of the relative abundances (%) of the ceramide chain lengths, labelled for each individual subclass, displayed for lesional AD.

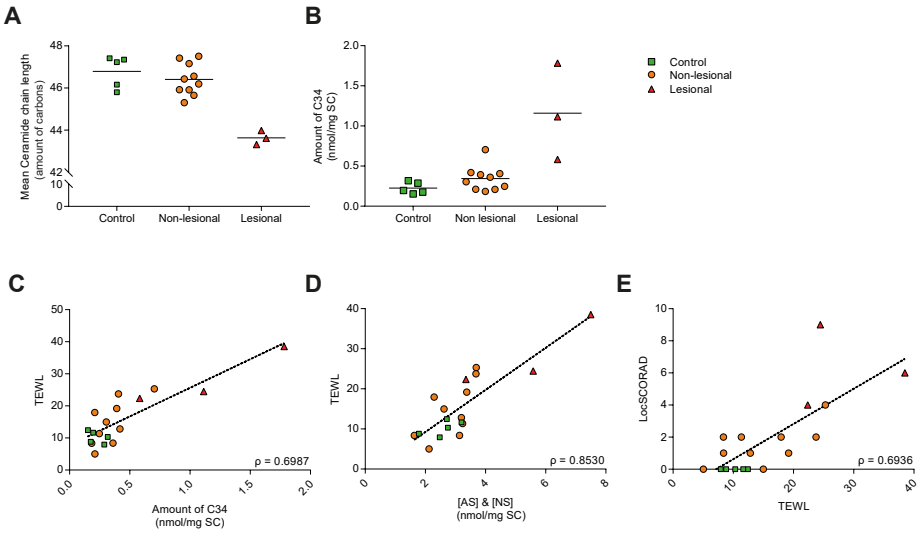

Supplemental figure S5: SC barrier lipid data. A. Dot plot of the mean ceramide chain length in the SC categorized by control, non-lesional or lesional AD skin. B. Dot plot of the absolute amount of C34 ceramides categorized by control, non-lesional or lesional AD skin. C. Dot plot TEWL and amount of C34 per subject. D. Dot plot TEWL and amount of ceramide [AS]&[NS] per subject E. Dot plot locSCORAD and TEWL per subject. All ρ's are calculated according to Spearman correlation test.

References

1. K.C. Madison, Barrier function of the skin: "la raison d'etre" of the epidermis, J Invest Dermatol, 121 (2003) 231-241.
2. P.M. Elias, M. Steinhoff, "Outside-to-inside" (and now back to "outside") pathogenic mechanisms in atopic dermatitis, J Invest Dermatol, 128 (2008) 1067-1070.
3. N.B. Silverberg, J.I. Silverberg, Inside out or outside in: does atopic dermatitis disrupt barrier function or does disruption of barrier function trigger atopic dermatitis?, Cutis, 96 (2015) 359-361.
4. P.M. Brunner, E. Guttman-Yassky, D.Y. Leung, The immunology of atopic dermatitis and its reversibility with broad-spectrum and targeted therapies, J Allergy Clin Immunol, 139 (2017) S65-S76.
5. C.N. Palmer, A.D. Irvine, A. Terron-Kwiatkowski, Y. Zhao, H. Liao, S.P. Lee, D.R. Goudie, A. Sandilands, L.E. Campbell, F.J. Smith, G.M. O'Regan, R.M. Watson, J.E. Cecil, S.J. Bale, J.G. Compton, J.J. DiGiovanna, P. Fleckman, S. Lewis-Jones, G. Arseculeratne, A. Sergeant, C.S. Munro, B. El Houate, K. McElreavey, L.B. Halkjaer, H. Bisgaard, S. Mukhopadhyay, W.H. McLean, Common loss-of-function variants of the epidermal barrier protein filaggrin are a major predisposing factor for atopic dermatitis, Nat Genet, 38 (2006) 441-446.
6. A.D. Irvine, W.H. McLean, Breaking the (un)sound barrier: filaggrin is a major gene for atopic dermatitis, J Invest Dermatol, 126 (2006) 1200-1202.
7. S. Kezic, A. Kammeyer, F. Calkoen, J.W. Fluhr, J.D. Bos, Natural moisturizing factor components in the stratum corneum as biomarkers of filaggrin genotype: evaluation of minimally invasive methods, Br J Dermatol, 161 (2009) 1098-1104.
8. G.M. O'Regan, A. Sandilands, W.H.I. McLean, A.D. Irvine, Filaggrin in atopic dermatitis, J Allergy Clin Immunol, 122 (2008) 689-693.
9. P.M. Elias, Structure and function of the stratum corneum extracellular matrix, J Invest Dermatol, 132 (2012) 2131-2133.
10. J.A. Bouwstra, F.E. Dubbelaar, G.S. Gooris, M. Ponec, The lipid organisation in the skin barrier, Acta Derm Venereol Suppl (Stockh), 208 (2000) 23-30.
11. J. van Smeden, J.A. Bouwstra, Stratum Corneum Lipids: Their Role for the Skin Barrier Function in Healthy Subjects and Atopic Dermatitis Patients, Curr Probl Dermatol, 49 (2016) 8-26.
12. K.R. Feingold, Thematic review series: skin lipids. The role of epidermal lipids in cutaneous permeability barrier homeostasis, J Lipid Res, 48 (2007) 2531-2546.
13. M. Rabionet, K. Gorgas, R. Sandhoff, Ceramide synthesis in the epidermis, Biochim Biophys Acta, 1841 (2014) 422-434.
14. K.R. Feingold, P.M. Elias, Role of lipids in the formation and maintenance of the cutaneous permeability barrier, Biochim Biophys Acta, 1841 (2014) 280-294.
15. S. Motta, M. Monti, S. Sesana, R. Caputo, S. Carelli, R. Ghidoni, Ceramide composition of the psoriatic scale, Biochim Biophys Acta, 1182 (1993) 147-151.
16. M. Janssens, J. van Smeden, G.S. Gooris, W. Bras, G. Portale, P.J. Caspers, R.J. Vreeken, T. Hankemeier, S. Kezic, R. Wolterbeek, A.P. Lavrijsen, J.A. Bouwstra, Increase in short-chain ceramides correlates with an altered lipid organization and decreased barrier function in atopic eczema patients, J Lipid Res, 53 (2012) 2755-2766.
17. J. Ishikawa, H. Narita, N. Kondo, M. Hotta, Y. Takagi, Y. Masukawa, T. Kitahara, Y. Takema, S. Koyano, S. Yamazaki, A. Hatamochi, Changes in the ceramide profile of atopic dermatitis patients, J Invest Dermatol, 130 (2010) 2511-2514.
18. J. van Smeden, M. Janssens, E.C. Kaye, P.J. Caspers, A.P. Lavrijsen, R.J. Vreeken, J.A. Bouwstra, The importance of free fatty acid chain length for the skin barrier function in atopic eczema patients, Exp Dermatol, 23 (2014) 45-52.
19. J. van Smeden, M. Janssens, G.S. Gooris, J.A. Bouwstra, The important role of stratum corneum lipids for the cutaneous barrier function, Biochim Biophys Acta, 1841 (2014) 295-313.
20. S. Ito, J. Ishikawa, A. Naoe, H. Yoshida, A. Hachiya, T. Fujimura, T. Kitahara, Y. Takema, Ceramide synthase 4 is highly expressed in involved skin of patients with atopic dermatitis, J Eur Acad Dermatol Venereol, 31 (2017) 135-141.
21. C.P. Shen, M.T. Zhao, Z.X. Jia, J.L. Zhang, L. Jiao, L. Ma, Skin Ceramide Profile in Children With Atopic Dermatitis, Dermatitis, 29 (2018) 219-222.
22. Y. Uchida, Ceramide signaling in mammalian epidermis, Biochim Biophys Acta, 1841 (2014) 453-462.
23. S. Hamanaka, M. Hara, H. Nishio, F. Otsuka, A. Suzuki, Y. Uchida, Human epidermal glucosylceramides are major precursors of stratum corneum ceramides, J Invest Dermatol, 119 (2002) 416-423.
24. Y. Uchida, M. Hara, H. Nishio, E. Sidransky, S. Inoue, F. Otsuka, A. Suzuki, P.M. Elias, W.M. Holleran, S. Hamanaka, Epidermal sphingomyelins are precursors for selected stratum corneum ceramides, J Lipid Res,

41 (2000) 2071-2082.
25. K. Jin, Y. Higaki, Y. Takagi, K. Higuchi, Y. Yada, M. Kawashima, G. Imokawa, Analysis of beta-glucocerebrosidase and ceramidase activities in atopic and aged dry skin, Acta Derm Venereol, 74 (1994) 337-340.
26. J.M. Jensen, R. Folster-Holst, A. Baranowsky, M. Schunck, S. Winoto-Morbach, C. Neumann, S. Schutze, E. Proksch, Impaired sphingomyelinase activity and epidermal differentiation in atopic dermatitis, J Invest Dermatol, 122 (2004) 1423-1431.
27. S. Kusuda, C.Y. Cui, M. Takahashi, T. Tezuka, Localization of sphingomyelinase in lesional skin of atopic dermatitis patients, J Invest Dermatol, 111 (1998) 733-738.
28. M. Danso, W. Boiten, V. van Drongelen, K. Gmelig Meijling, G. Gooris, A. El Ghalbzouri, S. Absalah, R. Vreeken, S. Kezic, J. van Smeden, S. Lavrijsen, J. Bouwstra, Altered expression of epidermal lipid bio-synthesis enzymes in atopic dermatitis skin is accompanied by changes in stratum corneum lipid composition, J Dermatol Sci, 88 (2017) 57-66.
29. J.P. Hachem, D. Crumrine, J. Fluhr, B.E. Brown, K.R. Feingold, P.M. Elias, pH directly regulates epidermal permeability barrier homeostasis, and stratum corneum integrity/cohesion, J Invest Dermatol, 121 (2003) 345-353.
30. Y. Hatano, M.Q. Man, Y. Uchida, D. Crumrine, T.C. Scharschmidt, E.G. Kim, T.M. Mauro, K.R. Feingold, P.M. Elias, W.M. Holleran, Maintenance of an acidic stratum corneum prevents emergence of murine atopic dermatitis, J Invest Dermatol, 129 (2009) 1824-1835.
31. I. Nomura, E. Goleva, M.D. Howell, Q.A. Hamid, P.Y. Ong, C.F. Hall, M.A. Darst, B. Gao, M. Boguniewicz, J.B. Travers, D.Y. Leung, Cytokine milieu of atopic dermatitis, as compared to psoriasis, skin prevents induction of innate immune response genes, J Immunol, 171 (2003) 3262-3269.
32. T. Kakinuma, K. Nakamura, M. Wakugawa, H. Mitsui, Y. Tada, H. Saeki, H. Torii, A. Asahina, N. Onai, K. Matsushima, K. Tamaki, Thymus and activation-regulated chemokine in atopic dermatitis: Serum thymus and activation-regulated chemokine level is closely related with disease activity, J Allergy Clin Immunol, 107 (2001) 535-541.
33. N. Furusyo, H. Takeoka, K. Toyoda, M. Murata, S. Maeda, H. Ohnishi, N. Fukiwake, H. Uchi, M. Furue, J. Hayashi, Thymus and activation regulated chemokines in children with atopic dermatitis: Kyushu University Ishigaki Atopic Dermatitis Study (KIDS), Eur J Dermatol, 17 (2007) 397-404.
34. E. Berdyshev, E. Goleva, I. Bronova, N. Dyjack, C. Rios, J. Jung, P. Taylor, M. Jeong, C.F. Hall, B.N. Richers, K.A. Norquest, T. Zheng, M.A. Seibold, D.Y. Leung, Lipid abnormalities in atopic skin are driven by type 2 cytokines, JCI Insight, 3 (2018).
35. Y. Hatano, H. Terashi, S. Arakawa, K. Katagiri, Interleukin-4 suppresses the enhancement of ceramide synthesis and cutaneous permeability barrier functions induced by tumor necrosis factor-alpha and interferon-gamma in human epidermis, J Invest Dermatol, 124 (2005) 786-792.
36. L.A. Gerbens, C.A. Prinsen, J.R. Chalmers, A.M. Drucker, L.B. von Kobyletzki, J. Limpens, H. Nankervis, A. Svensson, C.B. Terwee, J. Zhang, C.J. Apfelbacher, P.I. Spuls, i. Harmonising Outcome Measures for Eczema, Evaluation of the measurement properties of symptom measurement instruments for atopic eczema: a systematic review, Allergy, 72 (2017) 146-163.
37. H. Alexander, S. Brown, S. Danby, C. Flohr, Research Techniques Made Simple: Transepidermal Water Loss Measurement as a Research Tool, J Invest Dermatol, 138 (2018) 2295-2300 e2291.
38. S.G. Danby, M.J. Cork, pH in Atopic Dermatitis, Curr Probl Dermatol, 54 (2018) 95-107.
39. J.M. Hanifin, M. Thurston, M. Omoto, R. Cherill, S.J. Tofte, M. Graeber, The eczema area and severity index (EASI): assessment of reliability in atopic dermatitis. EASI Evaluator Group, Exp Dermatol, 10 (2001) 11-18.
40. Severity scoring of atopic dermatitis: the SCORAD index. Consensus Report of the European Task Force on Atopic Dermatitis, Dermatology, 186 (1993) 23-31.
41. Y. Uchida, The role of fatty acid elongation in epidermal structure and function, Dermatoendocrinol, 3 (2011) 65-69.
42. M.M. Man, K.R. Feingold, C.R. Thornfeldt, P.M. Elias, Optimization of physiological lipid mixtures for barrier repair, J Invest Dermatol, 106 (1996) 1096-1101.
43. A. Weerheim, M. Ponec, Determination of stratum corneum lipid profile by tape stripping in combination with high-performance thin-layer chromatography, Arch Dermatol Res, 293 (2001) 191-199.
44. C. Tawada, H. Kanoh, M. Nakamura, Y. Mizutani, T. Fujisawa, Y. Banno, M. Seishima, Interferon-gamma decreases ceramides with long-chain fatty acids: possible involvement in atopic dermatitis and psoriasis, J Invest Dermatol, 134 (2014) 712-718.
45. S. Borodzicz, L. Rudnicka, D. Mirowska-Guzel, A. Cudnoch-Jedrzejewska, The role of epidermal sphingolipids in dermatologic diseases, Lipids Health Dis, 15 (2016) 13.

46. J. van Smeden, I.M. Dijkhoff, R.W.J. Helder, H. Al-Khakany, D.E.C. Boer, A. Schreuder, W.W. Kallemeijn, S. Absalah, H.S. Overkleeft, J. Aerts, J.A. Bouwstra, In situ visualization of glucocerebrosidase in human skin tissue: zymography versus activity-based probe labeling, J Lipid Res, 58 (2017) 2299-2309.
47. J. van Smeden, H. Al-Khakany, Y. Wang, D. Visscher, N. Stephens, S. Absalah, H.S. Overkleeft, J.M.F.G. Aerts, A. Hovnanian, J.A. Bouwstra, Epidermal barrier lipid enzyme activity in Netherton patients relates with serine protease activity and stratum corneum ceramide abnormalities. Submitted.
48. W.A. Boiten, T. Berkers, S. Absalah, J. van Smeden, A.P.M. Lavrijsen, J.A. Bouwstra, Applying a vernix caseosa based formulation accelerates skin barrier repair by modulating lipid biosynthesis, J Lipid Res, 59 (2018) 250-260.
49. S. Seidenari, G. Giusti, Objective assessment of the skin of children affected by atopic dermatitis: a study of pH, capacitance and TEWL in eczematous and clinically uninvolved skin, Acta Derm Venereol, 75 (1995) 429-433.
50. F. Rippke, V. Schreiner, H.J. Schwanitz, The acidic milieu of the horny layer: new findings on the physiology and pathophysiology of skin pH, Am J Clin Dermatol, 3 (2002) 261-272.
51. R.J. Tamargo, A. Velayati, E. Goldin, E. Sidransky, The role of saposin C in Gaucher disease, Mol Genet Metab, 106 (2012) 257-263.
52. C.Y. Cui, S. Kusuda, T. Seguchi, M. Takahashi, K. Aisu, T. Tezuka, Decreased level of prosaposin in atopic skin, J Invest Dermatol, 109 (1997) 319-323.
53. W.M. Holleran, Y. Takagi, G.K. Menon, S.M. Jackson, J.M. Lee, K.R. Feingold, P.M. Elias, Permeability barrier requirements regulate epidermal beta-glucocerebrosidase, J Lipid Res, 35 (1994) 905-912.
54. E.B. Kelly, Encyclopedia of human genetics and disease, Greenwood, Santa Barbara, Calif., 2013.
55. R.W. Jenkins, D. Canals, Y.A. Hannun, Roles and regulation of secretory and lysosomal acid sphingomyelinase, Cell Signal, 21 (2009) 836-846.
56. J. Thijs, T. Krastev, S. Weidinger, C.F. Buckens, M. de Bruin-Weller, C. Bruijnzeel-Koomen, C. Flohr, D. Hijnen, Biomarkers for atopic dermatitis: a systematic review and meta-analysis, Curr Opin Allergy Clin Immunol, 15 (2015) 453-460.
57. D. Hijnen, M. De Bruin-Weller, B. Oosting, C. Lebre, E. De Jong, C. Bruijnzeel-Koomen, E. Knol, Serum thymus and activation-regulated chemokine (TARC) and cutaneous T cell- attracting chemokine (CTACK) levels in allergic diseases: TARC and CTACK are disease-specific markers for atopic dermatitis, J Allergy Clin Immunol, 113 (2004) 334-340.
58. Y. Kataoka, Thymus and activation-regulated chemokine as a clinical biomarker in atopic dermatitis, J Dermatol, 41 (2014) 221-229.
59. H. Tanojo, A. Bos-van Geest, J.A. Bouwstra, H.E. Junginger, H.E. Boodé, In vitro human skin barrier perturbation by oleic acid: Thermal analysis and freeze fracture electron microscopy studies, Thermochimica Acta, 293 (1997) 77-85.
60. E.G. Bligh, W.J. Dyer, A rapid method of total lipid extraction and purification, Can J Biochem Physiol, 37 (1959) 911-917.
61. W. Boiten, S. Absalah, R. Vreeken, J. Bouwstra, J. van Smeden, Quantitative analysis of ceramides using a novel lipidomics approach with three dimensional response modelling, Biochim Biophys Acta, 1861 (2016) 1652-1661.
62. J. van Smeden, W.A. Boiten, T. Hankemeier, R. Rissmann, J.A. Bouwstra, R.J. Vreeken, Combined LC/MS-platform for analysis of all major stratum corneum lipids, and the profiling of skin substitutes, Biochim Biophys Acta, 1841 (2014) 70-79.
63. M.D. Witte, W.W. Kallemeijn, J. Aten, K.Y. Li, A. Strijland, W.E. Donker-Koopman, A.M. van den Nieuwendijk, B. Bleijlevens, G. Kramer, B.I. Florea, B. Hooibrink, C.E. Hollak, R. Ottenhoff, R.G. Boot, G.A. van der Marel, H.S. Overkleeft, J.M. Aerts, Ultrasensitive in situ visualization of active glucocerebrosidase molecules, Nat Chem Biol, 6 (2010) 907-913.